Supplementary Information (SI) for Digital Discovery.

Supporting Information: Digital Workflow Optimization of van der Waals Methods for Improved Halide Perovskite Solar Materials

Celso R. C. Rêgo,[*,†] Maurício J. Piotrowski,[‡] Wolfgang Wenzel,[†] Alexandre C. Dias,[¶] Carlos Maciel de Oliveira Bastos,[§] Luís Octavio de Araújo,[‖] and Diego Guedes-Sobrinho[‖]

†*Institute of Nanotechnology Hermann-von-Helmholtz-Platz, Karlsruhe Institute of Technology, 76021 Karlsruhe, Germany*

‡*Department of Physics, Federal University of Pelotas, PO Box 354, 96010-900, Pelotas, RS, Brazil*

¶*Physical Institute, University of Brasília, Brasília, DF, 70919-970, Brazil*

§*São Carlos Institute of Physics, University of São Paulo, 13566-590, São Carlos–SP, Brazil*

‖*Chemistry Department, Federal University of Paraná, CEP 81531-980, Curitiba, Brazil*

E-mail: celso.rego@kit.edu

Table S1: Ionic radii (r_{ion}) for the X (N, P, As, and Sb), I, and Pb chemical elements, considering the respective charge state (CS) and coordination number (CN), from the literature.[1,2]

Element (Z)	Ion	CS	CN	r_{ion} (pm)
N (7)	N^{-3}	−3	4	146
P (15)	P^{-3}	−3	4	212
As (33)	As^{-3}	−3	4	222
Sb (51)	Sb^{-3}	−3	4	245
I (53)	I^{-1}	−1	6	220
Pb (82)	Pb^{+2}	2	6	119

Table S2: Pauling electronegativity for the chemical elements involved in the XH_4PbI_3 and $CH_3XH_3PbI_3$ (X = N, P, As, and Sb) constitution, from the literature.[3]

	H	C	N	P	As	Sb	I	Pb
Atomic number	1	6	7	15	33	51	53	82
Electronegativity	2.20	2.55	3.04	2.19	2.18	2.05	2.66	1.80

Table S3: For XH_4PbI_3: the tolerance factor, t, is obtained from the X−H average bond lengths, $d_{av,X-H}$, and the ionic radii of XH_4^+, r_{XH_4} (estimated by $r_{XH_4} = \sqrt{2}d_{av,X-H}$). For $CH_3XH_3PbI_3$: the t factor is obtained by two ways: (*i*) from the C−X bond lengths, d_{C-X}, and the ionic radii of $CH_3XH_3^+$, $r_{CH_3XH_3}$ (estimated by $r_{CH_3XH_3} = 0.5d_{C-X} + r_{X,ion}$); and (*ii*) from the distance between the center of mass (CM) of the molecule and the atom with the largest distance to CM, except the H atoms, d_{CM}, and the ionic radii of $CH_3XH_3^+$, $r_{CH_3XH_3}$ (estimated by $r_{CH_3XH_3} = d_{CM} + r_{X,ion}$). For both sets, X = N, P, As, and Sb, and all structures are optimized within empirical (D2, D3, and D3BJ), semi-empirical (TS, TSSCS, MBD, and dDsC), and without (std.) vdW corrections.

System		std.	D2	D3	D3BJ	TS	TSSCS	MBD	dDsC
NH_4PbI_3	$d_{av,N-H}$ (pm)	104.25	104.27	104.13	104.29	104.52	103.81	103.87	103.80
	r_{NH_4} (pm)	147.44	147.46	147.27	147.49	147.81	146.81	146.90	146.79
	t	0.7664	0.7665	0.7661	0.7665	0.7672	0.7651	0.7653	0.7651
PH_4PbI_3	$d_{av,P-H}$ (pm)	142.31	141.94	142.27	142.36	141.96	142.09	142.31	142.12
	r_{PH_4} (pm)	201.26	200.73	201.20	201.33	200.76	200.95	201.26	200.99
	t	0.8787	0.8776	0.8786	0.8788	0.8776	0.8780	0.8787	0.8781
AsH_4PbI_3	$d_{av,As-H}$ (pm)	152.20	151.51	151.88	152.19	151.77	152.02	152.20	151.84
	r_{AsH_4} (pm)	215.24	214.26	214.78	215.22	214.64	214.99	215.24	214.73
	t	0.9078	0.9058	0.9069	0.9078	0.9066	0.9073	0.9078	0.9068
SbH_4PbI_3	$d_{av,Sb-H}$ (pm)	170.41	169.85	170.37	170.48	169.96	170.09	169.70	169.31
	r_{SbH_4} (pm)	241.00	240.21	240.93	241.10	240.36	240.54	240.00	239.44
	t	0.9616	0.9599	0.9614	0.9618	0.9602	0.9606	0.9595	0.9583
System (by (*i*))		std.	D2	D3	D3BJ	TS	TSSCS	MBD	dDsC
$CH_3NH_3PbI_3$	d_{C-N} (pm)	149.11	149.32	148.97	148.96	149.10	149.02	148.97	148.87
	$r_{CH_3NH_3}$ (pm)	220.56	220.66	220.49	220.48	220.55	220.51	220.49	220.43
	t	0.9189	0.9192	0.9188	0.9188	0.9189	0.9188	0.9188	0.9187
$CH_3PH_3PbI_3$	d_{C-P} (pm)	179.49	179.45	179.43	179.50	179.21	179.21	179.42	179.23
	$r_{CH_3PH_3}$ (pm)	301.74	301.72	301.72	301.75	301.61	301.60	301.71	301.61
	t	1.0883	1.0882	1.0882	1.0883	1.0880	1.0880	1.0882	1.0880
$CH_3AsH_3PbI_3$	d_{C-As} (pm)	192.80	192.82	192.64	192.54	192.62	192.56	192.77	192.45
	$r_{CH_3AsH_3}$ (pm)	318.40	318.41	318.32	318.27	318.31	318.28	318.38	318.22
	t	1.1230	1.1230	1.1228	1.1228	1.1228	1.1228	1.1230	1.1227
$CH_3SbH_3PbI_3$	d_{C-Sb} (pm)	212.23	212.42	211.72	211.78	211.46	211.84	211.84	211.71
	$r_{CH_3SbH_3}$ (pm)	351.11	351.21	350.86	350.89	350.73	350.92	350.92	350.86
	t	1.2659	1.2662	1.2654	1.2655	1.2651	1.2655	1.2655	1.2654
System (by (*ii*))		std.	D2	D3	D3BJ	TS	TSSCS	MBD	dDsC
$CH_3NH_3PbI_3$	d_{CM} (pm)	78.64	79.44	79.25	79.24	78.64	78.62	78.58	78.53
	$r_{CH_3NH_3}$ (pm)	224.64	225.44	225.25	225.24	224.64	224.62	224.58	224.53
	t	0.9275	0.9291	0.9287	0.9287	0.9275	0.9274	0.9273	0.9272
$CH_3PH_3PbI_3$	d_{CM} (pm)	111.97	111.98	111.96	111.98	111.84	111.83	111.94	111.84
	$r_{CH_3PH_3}$ (pm)	323.97	323.98	323.96	323.98	323.84	323.83	323.94	323.84
	t	1.1346	1.1347	1.1346	1.1347	1.1344	1.1344	1.1346	1.1344
$CH_3AsH_3PbI_3$	d_{CM} (pm)	102.77	102.81	102.71	102.62	102.47	102.44	102.55	102.38
	$r_{CH_3AsH_3}$ (pm)	324.77	324.81	324.71	324.62	324.47	324.44	324.55	324.38
	t	1.1363	1.1364	1.1362	1.1360	1.1357	1.1356	1.1358	1.1355
$CH_3SbH_3PbI_3$	d_{CM} (pm)	70.40	70.50	70.13	70.16	69.99	70.20	70.20	70.22
	$r_{CH_3AsH_3}$ (pm)	315.40	315.50	315.13	315.16	314.99	315.20	315.20	315.22
	t	1.1168	1.1170	1.1162	1.1163	1.1159	1.1163	1.1163	1.1164

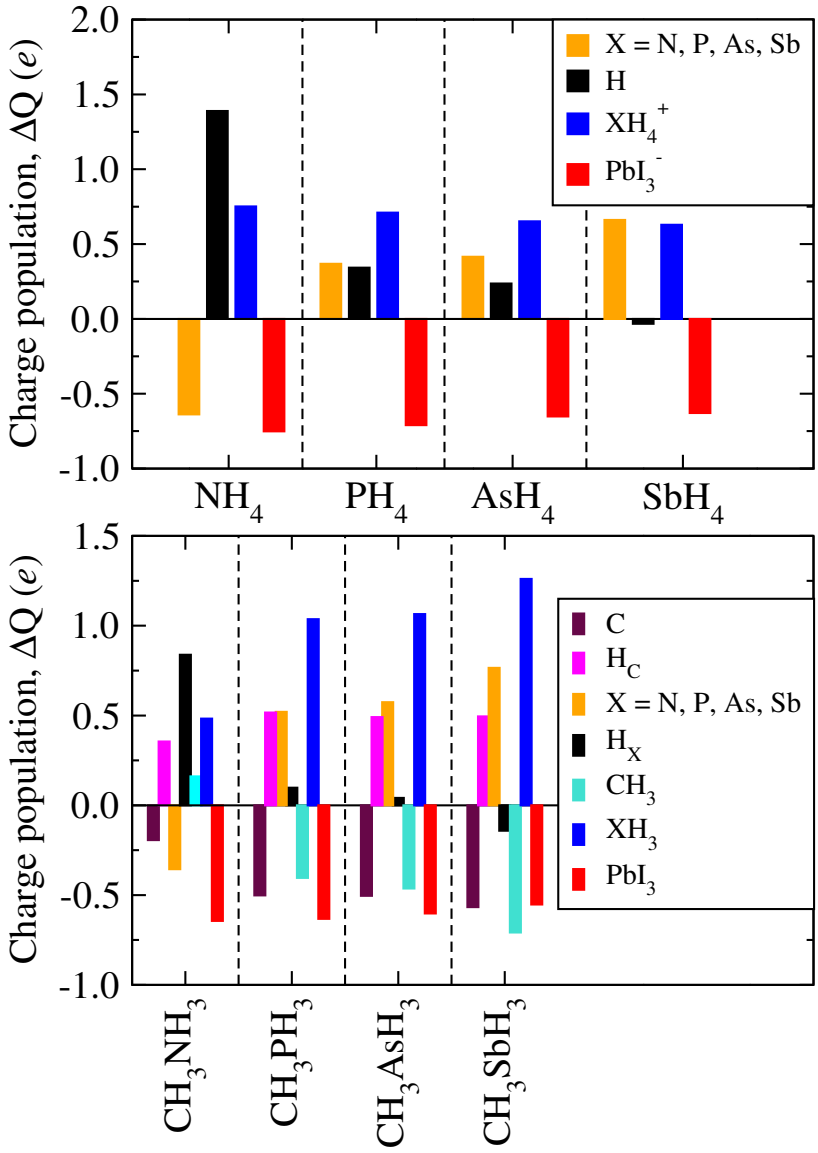

Figure S1: Partial charges computed for X (N, P, As, Sb), C, H_C, H_X, XH_4, CH_3, XH_3, and PbI_3 via density-derived electrostatic and chemical (DDEC6) method for the XH_4PbI_3 and $CH_3XH_3PbI_3$ MHPs.

The figure below illustrates the evaluation of various perovskite structures' structural distortion and electronic properties. The distortion in the perovskite octahedral unit is quantified using the Baur distortion index (D_i)[4,5], defined by $D_i = \frac{1}{6}\sum_{i=1}^{6}\left(\frac{|b_i-\bar{b}|}{\bar{b}}\right)$, where b_i represents the individual Pb bond lengths, and $\bar{b}$ is the average bond length across six bonds in the octahedron. A higher D_i value indicates significant distortion from an ideal symmetric octahedral configuration. The left side of the figure shows the D_i values calculated using different van der Waals (vdW) corrections for various perovskite structures, revealing that the degree of structural distortion is relatively low in these cases. The right side presents the corresponding band gap values (eV), reflecting variations in electronic properties across these structures and computational methods. The distortion index D_i supports the conclusion that Pb bonds do not play a major role in determining the band gaps of these materials, which is consistent with the lack of a clear trend between the D_i values and band gaps, suggesting that other factors, primarily the properties of the organic cations, dominate the band gap behavior in these systems.

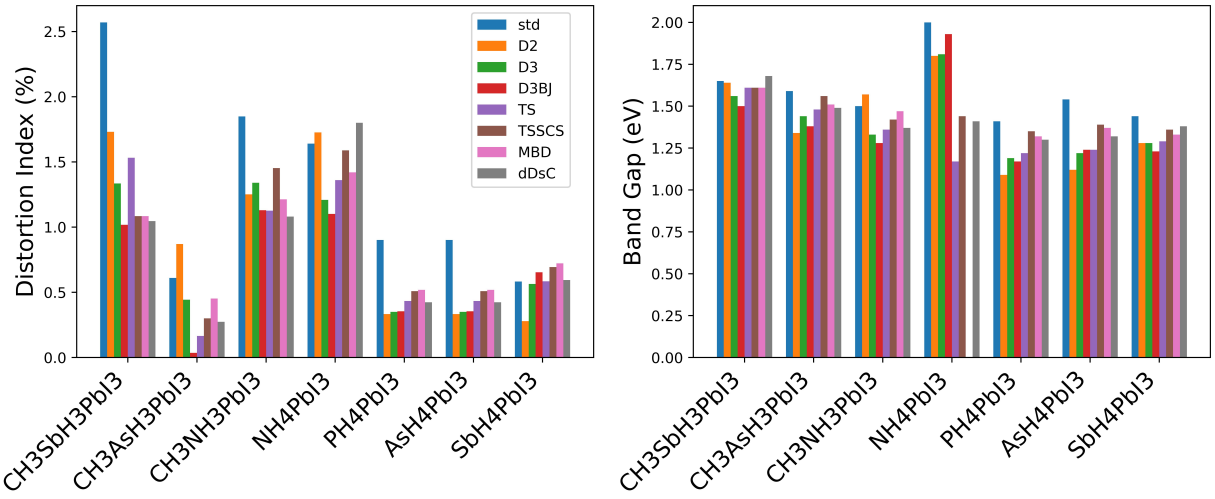

Figure S2: Bar plots comparing the distortion index (%) and band gap (eV) for various structures with different computational methods based on DFT-1/2+SOC. The left plot shows the distortion index, while the right plot displays the corresponding band gap values. Each bar group represents a specific structure (e.g., $CH_3SbH_3PbI_3$, $CH_3AsH_3PbI_3$, $CH_3NH_3PbI_3$, NH_4PbI_3, PH_4PbI_3 AsH_4PbI_3, and SbH_4PbI_3), and the bars within each group correspond to distinct methods, such as standard (std), D2, D3, D3BJ, TS, TSSCS, MBD, and dDsC.

Table S4: Equatorial (equat.) and apical (api.) Pb−I bonds and Pb−I−Pb angles as local structure parameters for XH_4PbI_3 (X = N, P, As, and Sb) perovskites obtained within empirical (D2, D3, and D3BJ), semi-empirical (TS, TSSCS, MBD, and dDsC), and without (std.) vdW corrections. The unit cell's α, β, and γ angles are indicated for every calculation mode.

Sys.	vdW	Pb−I bond (Å)		Pb−I−Pb angle (deg)		Unit cell (deg)		
		equat.	api.	equat.	api.	α	β	γ
NH_4PbI_3	std.	3.18–3.20	3.19–3.19	155–179	155–155	90	90	90
	D2	3.13–3.15	3.14–3.15	158–180	158–158	90	90	90
	D3	3.13–3.15	3.15–3.15	158–180	158–158	90	90	90
	D3BJ	3.14–3.15	3.14–3.16	154–178	154–154	90	90	91
	TS	3.07–3.17	3.16–3.16	169–179	179–179	90	90	89
	TSSCS	3.12–3.23	3.15–3.15	169–179	179–179	90	90	89
	MBD	3.10–3.21	3.13–3.13	167–179	178–178	90	90	89
	dDsC	3.11–3.20	3.12–3.12	167–179	178–178	90	90	89
		equat.	api.	equat.	api.	α	β	γ
PH_4PbI_3	std.	3.16–3.19	3.19–3.19	175–180	175–175	90	90	90
	D2	3.09–3.11	3.11–3.11	180–180	180–180	90	90	90
	D3	3.11–3.13	3.13–3.13	178–180	177–177	90	90	90
	D3BJ	3.10–3.12	3.12–3.12	176–180	176–176	90	90	90
	TS	3.10–3.16	3.14–3.14	179–180	179–179	90	90	90
	TSSCS	3.14–3.18	3.18–3.18	176–179	176–176	90	90	90
	MBD	3.12–3.15	3.15–3.16	173–180	173–173	90	90	90
	sDsC	3.12–3.15	3.15–3.15	175–179	174–174	90	90	90
		equat.	api.	equat.	api.	α	β	γ
AsH_4PbI_3	std.	3.16–3.21	3.20–3.22	172–178	169–169	90	90	90
	D2	3.09–3.12	3.10–3.12	178–179	180–180	90	90	90
	D3	3.10–3.15	3.14–3.15	178–180	177–177	90	90	90
	D3BJ	3.10–3.14	3.13–3.14	176–180	173–173	90	90	90
	TS	3.12–3.15	3.15–3.15	178–180	178–178	90	90	90
	TSSCS	3.13–3.20	3.19–3.19	174–178	175–178	90	90	90
	MBD	3.12–3.16	3.16–3.16	173–178	175–175	90	90	90
	dDsC	3.12–3.17	3.17–3.17	172–180	173–173	90	90	89
		equat.	api.	equat.	api.	α	β	γ
SbH_4PbI_3	std.	3.17–3.21	3.21–3.21	179–180	179–179	90	90	90
	D2	3.09–3.13	3.12–3.12	169–180	169–169	90	90	90
	D3	3.12–3.16	3.16–3.16	175–180	175–175	90	90	90
	D3BJ	3.10–3.14	3.14–3.14	174–180	174–174	90	90	89
	TS	3.11–3.16	3.16–3.16	175–180	175–175	90	90	90
	TSSCS	3.14–3.19	3.19–3.19	176–180	178–178	90	90	90
	MBD	3.11–3.16	3.16–3.16	172–179	172–172	90	90	90
	dDsC	3.12–3.16	3.16–3.16	170–180	170–170	90	90	90

Table S5: Equatorial (equat.) and apical (api.) Pb−I bonds and Pb−I−Pb angles as local structure parameters for $CH_3XH_3PbI_3$ (X = N, P, As, and Sb) perovskites obtained within empirical (D2, D3, and D3BJ), semi-empirical (TS, TSSCS, MBD, and dDsC), and without (std.) vdW corrections. The α, β, and γ angles of the unit cell are indicated for every calculation mode.

Sys.	vdW	Pb−I bond (Å)		Pb−I−Pb angle (deg)		Unit cell (deg)		
		equat.	api.	equat.	api.	α	β	γ
$CH_3NH_3PbI_3$	std.	3.07–3.35	3.20–3.27	168–172	169–169	90	89	90
	D2	3.06–3.25	3.13–3.13	160–164	160–160	90	89	90
	D3	3.08–3.22	3.16–3.19	168–172	172–172	90	89	90
	D3BJ	3.07–3.20	3.15–3.18	168–172	172–172	90	90	90
	TS	3.06–3.30	3.18–3.21	170–174	169–169	90	88	90
	TSSCS	3.04–3.37	3.20–3.24	171–176	169–169	90	89	90
	MBD	3.06–3.30	3.19–3.23	166–171	170–170	90	89	90
	dDsC	3.10–3.23	3.18–3.21	168–172	171–171	90	89	90
		equat.	api.	equat.	api.	α	β	γ
$CH_3PH_3PbI_3$	std.	3.21–3.22	3.23–3.23	179–179	180–180	90	87	90
	D2	3.15–3.16	3.13–3.13	178–180	179–179	90	87	90
	D3	3.16–3.18	3.15–3.17	179–179	180–180	90	87	90
	D3BJ	3.15–3.16	3.15–3.16	179–179	180–180	90	88	90
	TS	3.18–3.20	3.19–3.19	180–180	180–180	90	86	90
	TSSCS	3.20–3.22	3.21–3.21	180–180	180–180	90	86	90
	MBD	3.18–3.20	3.18–3.18	180–180	180–180	90	86	90
	dDsC	3.18–3.20	3.17–3.17	180–180	180–180	90	86	90
		equat.	api.	equat.	api.	α	β	γ
$CH_3AsH_3PbI_3$	std.	3.19–3.26	3.24–3.25	177–177	177–177	90	86	90
	D2	3.13–3.18	3.14–3.14	178–178	180–180	90	84	90
	D3	3.14–3.22	3.16–3.20	177–178	179–179	90	85	90
	D3BJ	3.13–3.19	3.15–3.17	177–178	180–180	90	85	90
	TS	3.20–3.22	3.20–3.20	177–178	180–180	90	85	90
	TSSCS	3.21–3.23	3.23–3.23	180–180	180–180	90	86	90
	MBD	3.19–3.21	3.20–3.20	180–180	180–180	90	85	90
	dDsC	3.19–3.21	3.19–3.19	180–180	180–180	90	85	90
		equat.	api.	equat.	api.	α	β	γ
$CH_3SbH_3PbI_3$	std.	3.26–3.30	3.25–3.25	176–178	177–177	90	86	90
	D2	3.16–3.21	3.10–3.23	171–175	165–165	90	83	90
	D3	3.20–3.26	3.14–3.23	174–180	173–173	90	84	90
	D3BJ	3.18–3.23	3.13–3.19	174–179	173–173	90	84	90
	TS	3.14–3.30	3.14–3.26	175–179	171–171	90	84	90
	TSSCS	3.19–3.26	3.17–3.23	170–177	174–174	90	85	90
	MBD	3.19–3.26	3.17–3.23	170–177	174–174	90	85	90
	dDsC	3.18–3.25	3.16–3.23	171–172	168–168	90	84	90

References

(1) Pauling, L. *The Nature of the Chemical Bond*; Cornell University Press: Ithaca, 1960.

(2) Shannon, R. D. Revised effective ionic radii and systematic studies of interatomic distances in halides and chalcogenides. *Acta Crystallogr., Sect. A: Found. Crystallogr.* **1976**, *32*, 751–767.

(3) Haynes, W. M. *CRC Handbook of Chemistry and Physics, 95th Edition*; Taylor & Francis Group, 2014.

(4) Baur, W. H. The geometry of polyhedral distortions. Predictive relationships for the phosphate group. *Acta Crystallographica Section B Structural Crystallography and Crystal Chemistry* **1974**, *30*, 1195–1215.

(5) Morteza Najarian, A.; Dinic, F.; Chen, H.; Sabatini, R.; Zheng, C.; Lough, A.; Maris, T.; Saidaminov, M. I.; García de Arquer, F. P.; Voznyy, O.; Hoogland, S.; Sargent, E. H. Homomeric chains of intermolecular bonds scaffold octahedral germanium perovskites. *Nature* **2023**, *620*, 328–335.